The zero-moment half metal: How could it change spin electronics?

Davide Betto, Karsten Rode' , Naganivetha Thiyagarajah' , Yong-Chang Lau, Kiril Borisov, Gwenael Atcheson, Mario Žic, Thomas Archer, Plamen Stamenov, and J. M. D. Coey

Citation: AIP Advances **6**, 055601 (2016); doi: 10.1063/1.4943756
View online: http://dx.doi.org/10.1063/1.4943756
View Table of Contents: http://aip.scitation.org/toc/adv/6/5
Published by the American Institute of Physics

The zero-moment half metal: How could it change spin electronics?

Davide Betto,[1] Karsten Rode,[1,a] Naganivetha Thiyagarajah,[1,b] Yong-Chang Lau,[1] Kiril Borisov,[1] Gwenael Atcheson,[1] Mario Žic,[2] Thomas Archer,[2] Plamen Stamenov,[1] and J. M. D. Coey[1]
[1]*CRANN, AMBER and School of Physics, Trinity College Dublin, Dublin 2, Ireland*
[2]*CRANN, and School of Physics, Trinity College Dublin, Dublin 2, Ireland*

(Presented 12 January 2016; received 6 November 2015; accepted 8 January 2016; published online 7 March 2016)

The Heusler compound Mn_2Ru_xGa (MRG) may well be the first compensated half metal. Here, the structural, magnetic and transport properties of thin films of MRG are discussed. There is evidence of half-metallicity up to $x = 0.7$, and compensation of the two Mn sublattice moments is observed at specific compositions and temperatures, leading to a zero-moment half metal. There are potential benefits for using such films with perpendicular anisotropy for spin-torque magnetic tunnel junctions and oscillators, such as low critical current, high tunnel magnetoresistance ratio, insensitivity to external fields and resonance frequency in the THz range. [http://dx.doi.org/10.1063/1.4943756]

I. INTRODUCTION

Half metals are ideal ferromagnets with a spin gap in the majority or minority density of states.[1,2] As a consequence, they exhibit a spin moment per stoichiometric formula unit that is an integral number of Bohr magnetons. The conduction electrons are perfectly spin polarized. Such an ideal material is obviously of interest for spin electronics,[3] where high spin polarization is associated with large magnetoresistance in sensors and memory elements and with a high spin transfer torque efficiency in magnetic switches and oscillators. However, the ideal of 100% spin polarization is never achieved in practice. Spin-orbit coupling inevitably mixes ↑ and ↓ states,[4] certain antisite disorder destroys half metallicity[5] and thermal excitation reduces the spin polarization.[2] Furthermore, the effective spin polarization in device structures is largely determined by a few layers near the interface where the electronic structure often differs from the bulk.

The half metals that have had the greatest impact on spin electronics so far have been cobalt-based Heusler alloys with a high Curie temperature. Co_2MnSi (T_C = 985 K) and $Co_2FeAl_{0.5}Si_{0.5}$ (T_C = 1150 K)[6] have been incorporated into magnetic tunnel junctions with MgO barriers that exhibit a tunnel magnetoresistance which approaches 1000% at low temperature.[7,8] These alloys are useful for current-perpendicular-to-plane GMR read heads for high-density magnetic recording.[3]

No single element is a half metal. Structurally, the simplest is the ferromagnetic binary oxide CrO_2, which has the rutile structure with a moment of 2 μ_B f.u.$^{-1}$ and chromium in a single site.[9] The spin gap is between the O(2*p*) band and the unoccupied Cr minority-spin 3*d* band. A moment of 0 μ_B is impossible with a single magnetic sublattice, but it becomes possible when there are two (or more). When the two sublattices are chemically and crystallographically equivalent and oppositely directed, we have an antiferromagnet, where no unbalanced spin polarization is possible. There must be equal densities of ↑ and ↓ electrons at the Fermi level at least in the bulk, although the appropriate surfaces of a planar antiferromagnet can be spin polarized.

[a]Corresponding author: rodek@tcd.ie
[b]Current address: Globalfundries, Singapore, 60 Woodlands Industrial Park D Street 2, Singapore 738406

An interesting possibility arises for metals with crystallographically inequivalent magnetic sublattices. The sublattice moments may be antiparallel in a ferrimagnetic structure, and it is possible that they precisely compensate each other. The ferrimagnet can be half-metallic if there is a spin gap in the total density of states, and there is nothing in principle that prevents magnetic order with a net spin moment of 0 μ_B.[10] Such material is called 'compensated ferrimagnetic half metal' or a 'zero-moment half metal'. There have been many suggestions for candidate materials,[11] especially among the Heusler compounds, but generally they turned out to be unstable, nonmagnetic, or crystallized in a different structure with no spin gap. Almost all of the predicated candidates contain Mn, exploiting its high and localised magnetic moment.[12] The first experimental evidence for the existence of the long-sought material came in 2014, with the synthesis of near-cubic thin films of $Mn_2Ru_{0.5}Ga$ (MRG).[13]

Reality is rarely perfect, and real half metals are messier than the ideal. Complete compensation only occurs at a single temperature, $T = 0$ K, because the two inequivalent sublattices experience different exchange interactions and their sublattice magnetizations have different temperature dependences.[14] The compensation may be adjusted to be close to room temperature by a slight change of composition, but this can be detrimental to spin polarization unless the spin gap is wide. It has been difficult to obtain compelling experimental evidence for half-metallicity, especially with surface-sensitive measurements.[2] Nevertheless, the possible combination of high spin polarization and zero magnetization is a tantalizing one, which is well worth exploring, both practically and imaginatively. This is our objective here.

II. GROWTH AND STRUCTURE

MRG films with different Ru content are grown on MgO (001) substrates by DC magnetron sputtering at 250 °C substrate temperature in a Shamrock system with a base pressure of 2×10^{-8} Torr. They were co-sputtered from Ru and stoichiometric Mn_2Ga targets. The Ru concentration was controlled by varying the Mn_2Ga target plasma power while fixing the Ru one. The samples were then capped with a protective layer of 2 nm of Al_2O_3.

X-ray diffraction data are presented in Fig. 2. The value of the in-plane lattice parameter a was determined by reciprocal space mapping (RSM) and was always consistent with the value of 595.6 pm = $\sqrt{2}a_{MgO}$, meaning that Mn_2Ru_xGa grows on MgO with its unit cell rotated by an angle of 45°. The out-of-plane parameter c is found to be between 598 pm and 618 pm, depending on the Ru concentration and the film thickness; c increases sharply with reducing film thickness. This confirms the essentially cubic character of the MRG films, with a slight tetragonal distortion ($[c - a]/a = \Delta c/a$ between 1.8% and 3.6%). Interestingly, as the film thickness is varied, the substrate-induced strain is non-volume-conserving, indicating that another mechanism may be at least partly responsible for the stabilisation of the half-metallic cubic structure. This observation will be discussed in section IV.

As the crystal evolves from a $C1_b$ structure (half Heusler) to the $L2_1$ structure (inverse full Heusler) (Fig. 1), Mn atoms occupy the inequivalent 4*a* and 4*c* positions, while Ga atoms occupy the 4*b* position. Ru atoms increasingly fill the empty 4*d* positions as x increases. Therefore, the 4*a* Mn at the corner of a big MnGa cube is octahedrally coordinated by Ga, while the Mn in the 4*c* position is octahedrally coordinated by Ru and tetrahedrally coordinated by both 4*a* Mn and 4*b* Ga.

The degree of ordering of different elements can be evaluated by analysis of the (115) reflection and by the relative intensities of the (002) and (004) reflections. Rietveld simulations of the peak intensities shows that the (115) peak is directly related to in-plane ordering between 4*a* Mn and 4*b* Ga and between 4*c* Mn and 4*d* Ru. For optimum growth conditions, the relative intensity of this reflection reaches $\simeq 0.35$, indicating a high degree of in-plane ordering. Similarly, Rietveld analysis shows that the ratio of the intensities of the (002) and (004) peaks is related to ordering across planes in the crystal structure; the higher the (002)/(004) ratio, the less ordered the structure, with interchange between 4*a* Mn and 4*d* Ru and between 4*c* Mn and 4*b* Ga. Again, for optimised growth conditions, we obtain high degree of ordering across planes, with an intensity ratio as low as 0.1. Results as a function of the growth temperature are shown in Fig. 3, together with the full-width at half-maximum (FWHM) of the rocking curve of the main peak in the $L2_1$ cubic structure. The

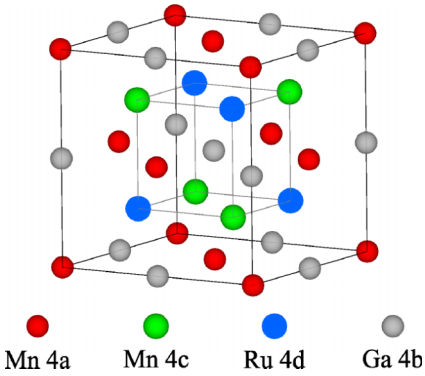

FIG. 1. $L2_1$ crystal structure of MRG.

FWHM of the symmetric reflection gives an estimate of the crystalline quality of the film: peaks that are broadened solely by crystallite size are indicative of a low spread of the c parameter, whereas the FWHM of the rocking curve reflects the degree of mosaicity.

The degree of tetragonal distortion, which is critical for perpendicular magnetic anisotropy, can be controlled by varying the film thickness. We prepared MRG with the same Ru concentration ($x \approx 1.0$), while varying the thickness from 70 nm down to 4 nm. The absence of structure around the symmetric (204) reflection indicates that there is negligible variation of the strain across the film thickness. The mosaicity of the MgO substrate impedes a quantitative estimation of the variation of the c parameter across the thickness.

The magnetisation and magnetic anisotropy vary remarkably with Ru concentration. The magnetic moment decreases steadily with x until it reaches practically zero for $x \sim 0.6$ and then increases again, as shown in Fig. 4. After our first paper,[13] we improved our knowledge of the sample composition; therefore, the values of x where the compensation occurs is slightly different from previously published. We infer that this behaviour is due to a change of sign of the magnetisation. There is a large increase of hysteresis where the magnetisation crosses zero, whether as a function of x or T. For Mn_2Ga, $x = 0$, the Fermi level is a few hundreds of meV below the spin gap $\Delta_\downarrow$ in the $\downarrow$ band. In a rigid-band approximation, the addition of Ru shifts the Fermi level inside the spin gap by adding both electrons and states. MRG loses its half-metallicity again when the Ru content is high enough to move the Fermi level above the spin gap. According to the Slater-Pauling rules,[15] cubic Mn_2Ga and Mn_3Ga should have a moment of $-1\ \mu_B$ f.u.$^{-1}$ and $+1\ \mu_B$ f.u.$^{-1}$ respectively. The slope of $2\ \mu_B$ f.u.$^{-1}$ found in the region $0.3 < x < 0.7$ is the primary evidence that MRG is a half metal.

The spin polarisation at the Fermi level therefore changes sign with respect to the net magnetisation with increasing x. The same effect can be achieved by changing the temperature: the two magnetic sublattices show different temperature dependence of their magnetisation. Therefore, as the temperature is varied, the magnetisation switches sign at the compensation point.

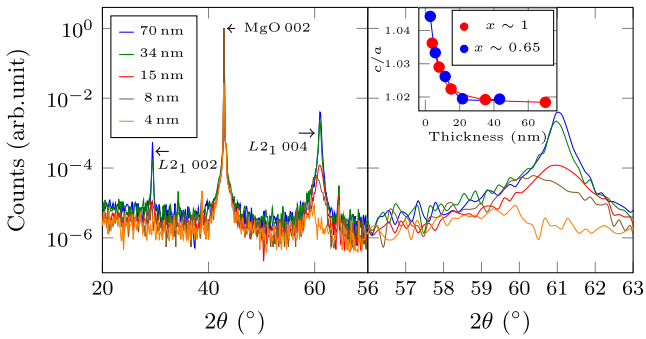

FIG. 2. Left: XRD pattern of $L2_1$ Mn_2Ru_xGa grown on a MgO (001) substrate varying film thickness. Right: MRG (004) peak varying film thickness. Inset: Tetragonal distortion c/a varying film thickness.

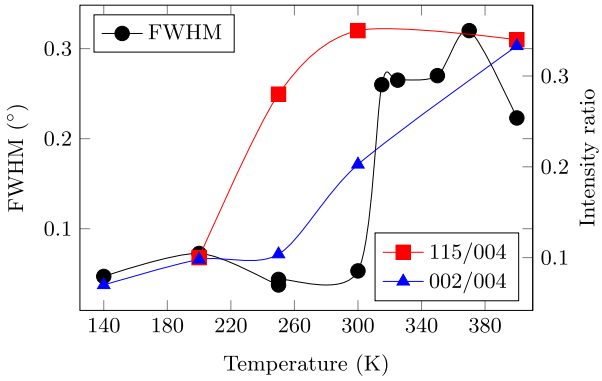

FIG. 3. FWHM of the 004 rocking curve, and intensities of the 115 and 002 peaks relative to the 004 peak as a function of the deposition temperature.

III. MAGNETIC AND ELECTRONIC PROPERTIES

Site-specific magnetic properties were studied by recording XAS spectra on the Mn $L_{3,2}$ edges in a field of $\mu_0 H = 6.8$ T with the sample normal parallel to both the field and the X-ray propagation vector $\vec{k}$. No absorption was seen in the energy range corresponding to Ga $L_{3,2}$ edges, indicating that Ga is close to a $3d^{10}$ configuration with no final states available in the $3d$ band. The signal to noise ratio on the Ru $M_{3,2}$ edges was too poor to obtain any magnetic or structural information.

Despite the overlapping absorption from the two Mn sites, it was possible to extract information on the Mn moments[16] by direct comparison with an explicit quantum mechanical core-hole-corrected multiplet calculation. The magnetic moments are then given by the calculated expectation values of $\langle S_z \rangle$ and $\langle L_z \rangle$, obtained by scaling the calculated dichroic signal to the observed XMCD.[17]

Fig. 5 shows the calculated and measured contributions from the two, antiferromagnetically coupled sites. Zero-temperature expectation values $2\langle S_z \rangle$ of $4.35\mu_B$ and $4.85\mu_B$ with $3d$ occupation numbers of 5.65 and 5.15 were found for the $4a$ and $4c$ positions, respectively. The orbital momentum $\langle L_z \rangle$ and the dipolar moment $\langle T_z \rangle$ are negligible for both positions, as expected for a $3d^5$ configuration. Comparison of the values of $2\langle S_z \rangle$ with recent neutron diffraction measurements[18]

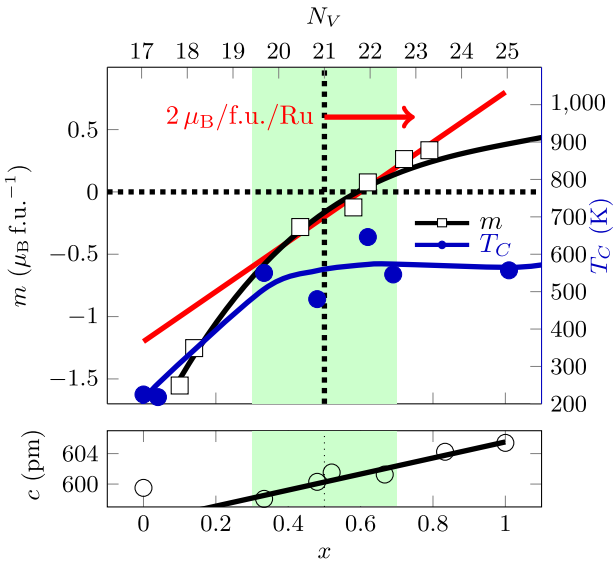

FIG. 4. Variation of Curie temperature T_C and moment with Ru concentration x and number of valence electrons per formula unit N_v. The half-metallic region is lightly shaded. The lower panel shows the variation of the lattice parameter c, normal to the substrate, as a function of x. After Ref. 13.

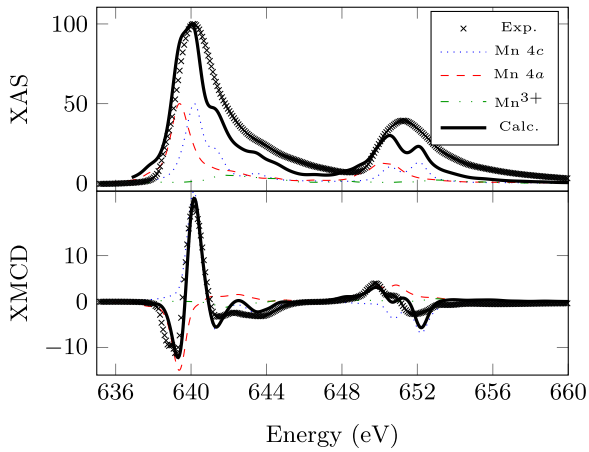

FIG. 5. The isotropic X-ray absorption and dichroism spectra for a typical Mn_2Ru_xGa sample. The calculated contribution from each crystallographic position is shown in thin dotted/dashed lines. The dichroic spectra for each site has opposite sign for the two positions $4a$ and $4c$, confirming their antiferromagnetic coupling. After Ref. 17.

and DFT calculations[19] indicates that they are likely to be about 30% too high. Nevertheless , they are resolved and of opposite sign.

There is an evident variation of the magnitudes of the moments of MRG samples with different x and c/a ratio. The $4c$ magnetisation decreases almost linearly with temperature; the extrapolated Curie temperature T_C of $\sim$ 550 K is in good agreement with the results of neutron diffraction on bulk powders of Mn_2RuGa.[20] By contrast, the $4a$ magnetisation is almost constant below and around room temperature. Hence the magnetisation switches at a temperature that depends on both x and the degree of strain. For thick films (low substrate-induced strain), we found the compensation occurs at $x \approx 0.6$, in agreement with the revised magnetometry data (Fig. 4 and Fig. 6).

Extrapolating the magnetic moments to $T = 0$ K, we can investigate the evolution of the absolute value of $2\langle S \rangle$ at $4a$ and $4c$ positions as a function of x (Fig. 6). Since the former is almost constant, we conclude that the electronic band edges originating from Mn occupying this crystallographic position are not reached by the Fermi level. The large spread of values is due to the varying c/a ratio; the average spin moment is 0.68 μ_B.

On the other hand, the $4c$ moment increases sharply in the range $0.60 < x < 0.75$, causing a change of the sign of the net moment near $x = 0.65$. For $x > 0.75$ we identify a second region, where the $4c$ magnetisation increases moderately up to $x = 1.2$. In our interpretation, the addition

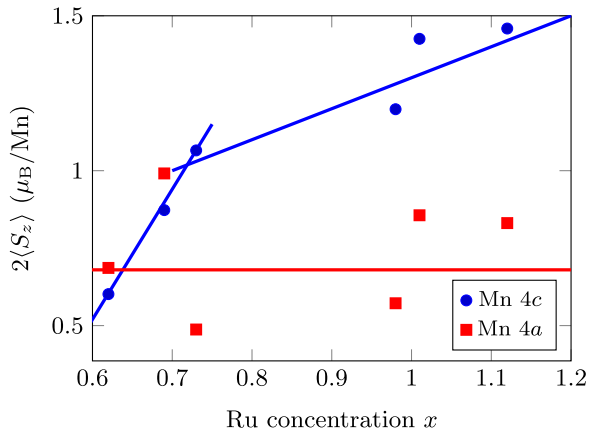

FIG. 6. Evolution of the absolute value of the magnetic moments at of the two Mn positions, extrapolated to $T = 0$ K, with Ru concentration x. The solid lines are linear regressions to the data sets. In the case of Mn $4c$, we identify a change of slope in the vicinity of $x = 0.7$, corresponding to the onset of filling the minority spin channel of Mn in this position. After Ref. 17.

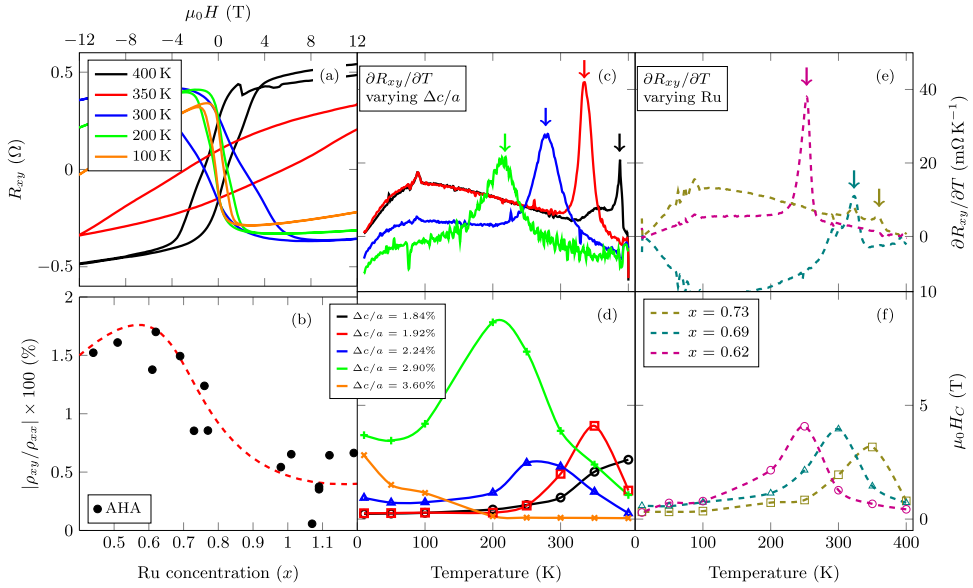

FIG. 7. (a) Spontaneous Hall effect of Mn_2Ru_xGa with $\Delta c/a = 1.92\%$ at different temperatures. The hysteresis loops have been centered at $R_{xy} = 0$. The legend in (f) is common to panels (c)-(f). (b) Anomalous Hall angle (AHA) as a function of Ru concentration x, as extracted from AHE measurements at 300 K. The lines are a guide to the eye. (c) - (f) Temperature dependent transport properties of two sets of samples; (c) and (d): with the same Ru concentration ($x \sim 1.0$) and varying $\Delta c/a$ (between 1.8% and 3.6%). (e) and (f): with the same $\Delta c/a$ (~ 1.9) and varying Ru concentration x (between 0.62 and 0.73). Panels (c) and (e) show the temperature derivative of the Hall resistance, with a maximum at T_{comp} , while (d) and (f) trace the temperature evolution of their coercive fields. T_{comp} is indicated by the arrows in panels (c) and (e). After Ref. 23.

of Ru results in the hybridization of the band structure originating from the 4*c* position, leading to the displacement of the latter towards the Fermi level and a corresponding variation of magnetic moment. The slope of this variation is related to the fine structure of the band, resulting in an abrupt change in the 4*c* spin ↑ occupied density of states at $x \sim 0.7$ (Fig. 4).

The anomalous Hall voltage[21,22] has been measured for a series of samples with thickness 70 nm and therefore very similar values of $\Delta c/a$ ~1.9%.[23] The Hall resistance changes sign at $x \sim 0.69$, confirming the change of sign of spin polarisation with respect to the applied external field.

In Fig. 7(a) we show the anomalous Hall resistance of an MRG sample with $x = 1$ and $\Delta c/a$ =1.92%. The AHE has been measured at different temperatures and it changes sign between 300 and 350 K, where the hysteresis becomes very large, due to the diverging anisotropy field. We found that the compensation temperature T_{comp} moves to lower temperature as x is lowered. This reflects the temperature dependence of the Mn 4*c* sublattice as a function of Ru concentration.

From the AHE loops, it is also clear that the coercive field H_c impedes complete saturation when approaching T_{comp}, since the anisotropy field $\mu_0 H_{\text{an}} = 2K_u/M_s$ diverges when M_s goes to zero.

Fig. 7(c) shows the temperature derivative of the AHE resistance $\partial R_{xy}/\partial T$ as a function of temperature series of samples with same x but different $\Delta c/a$. The compensation temperature shifts to lower values as the tetragonal distortion is increased. Fig. 7(d) shows the corresponding variation of the coercive field H_c, diverging at T_{comp}.

The anomalous Hall angle (AHA) is defined as the ratio ρ_{xy}/ρ_{xx}. Fig. 7(b) shows its evolution with x. The value is almost constant in temperature, therefore we used the data taken at 300 K for the analysis. The longitudinal resistivity ρ_{xx} is not shown since it is almost constant over the whole range. The measured AHA of ~ 1.7% in the half-metallic region is about an order of magnitude higher than usual for 3*d* ferromagnets (0.2% to 0.3%),[24] and similar to values measured in rare earth transition metal alloys[25] and dilute magnetic semiconductors.[26,27] Such a large AHE is a symptom of a low carrier concentration and a high spin polarisation. Since the AHA increases with decreasing Ru concentration, it cannot be due to the spin-orbit scattering coming from the number of Ru atoms.

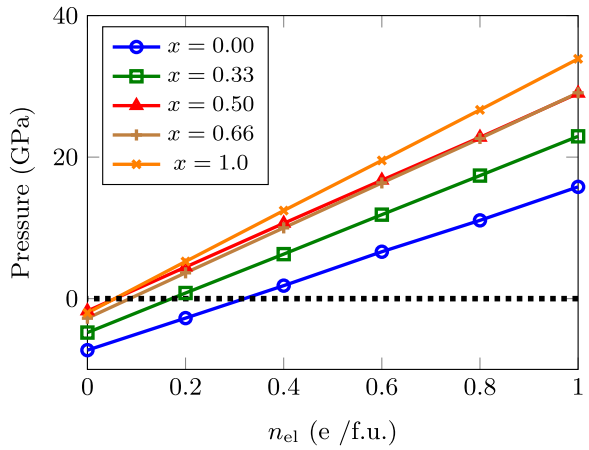

FIG. 8. Calculated pressure for cubic MRG films with fixed lattice parameter, corresponding to the experimentally determined a value, as a function of electron doping n_{el}. After Ref. 28.

In addition, changes in electronic mobility and carrier concentration effects the Hall voltage but not the AHA. Therefore, we infer an extremely high intrinsic contribution to the Hall scattering and/or a very high spin polarisation at the Fermi level, as is the case in Mn:GaAs.

IV. ELECTRONIC STRUCTURE

Mn_2Ru_xGa compounds have been investigated by density functional theory (DFT) calculations.[28] While confirming the possibility of realising a zero-moment compound, the simulations suggest it would not be a half metal. Nevertheless, $Mn_2Ru_{0.5}Ga$ has very large spin polarisation, which appears as a "pseudo-gap" at the Fermi level. Although the "pseudo-gap" may tentatively explain the spin-polarization in transport measurements; it cannot account for the anomalous strain, where we observe the in-plane lattice parameter a constrained by the MgO substrate while the out-of-plane parameter c varies with the film thickness, resulting in a non-volume-conserving strain. In addition, the DFT calculations do not agree with the measured magnetic moment as a function of x,[29] as shown in Fig. 10.

Further DFT investigations of alternative stoichiometry in the Mn, Ga and Ru containing Heuslers demonstrate the presence of several phases close in energy which differ from the $Mn_2Ru_{0.5}Ga$ structure by substitution on the 4a site as shown in Fig. 9 with $MnGa_2Ru$ being the lowest energy phase. The energy difference between these competing phases is not sufficient to justify phase segregation

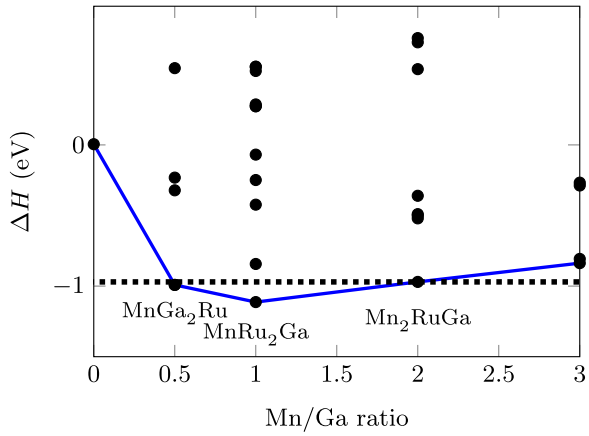

FIG. 9. High-throughput MnGa phase diagram. After Refs. 28 and 30.

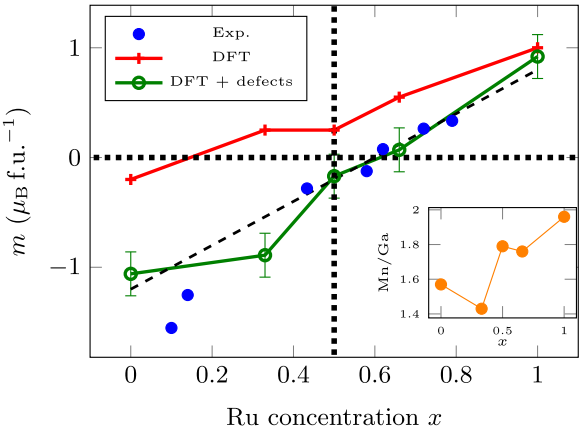

FIG. 10. Comparison of the experimental magnetic moment with the predicted moment within the DFT, with and without defects. Inset: corresponding estimate of the Mn/Ga ratio. After Ref. 28.

but instead we expect site disorder on the $4a$ site favouring lower Mn content. Mass spectrometry measurements on our films confirm that the Mn/Ga ratio does indeed favour lower Mn content.[30]

Substituting Ga for Mn provides a significant source of electronic doping which results in the anomalous strain observed. Fig. 8 shows the pressure as a function of the electronic doping n_{el} for a compound with lattice parameter fixed at the experimentally determined a value. It is clear that electronic doping provides the internal forces necessary to stabilise the MRG thin films in the pseudo-cubic structure. In addition, the measured magnetic moment as a function of x can only be explained when Mn/Ga substitutions are considered. Fig. 10 shows the estimated moments with and without the inclusion of these defects in the simulations. The latter results are in fair agreement with the experimental data and reproduce the slope of 2 μ_B f.u.$^{-1}$. Interestingly, electronic doping of 1 electron/f.u. in $Mn_2Ru_{0.5}Ga$ restores the half-metallic ground state. To achieve transport half-metallicity and zero net moment at room temperature, a reduced Mn/Ga ratio of ≈ 1.4 is required, together with a Ru concentration of ≈ 0.7.

V. CONCLUSIONS

The study of MRG thus far has revealed some characteristic features of compensated ferrimagnetic thin films, namely the divergence of the anisotropy field and hysteresis at the compensation point, when the films have some perpendicular anisotropy to begin with. The perpendicular anisotropy K_1 deduced from EHE and magnetization measurements in pseudocubic films far from compensation is ≈ 30 kJ m^{-3}, and it can be controlled by biaxial strain. High-field magnetization measurements have been used to deduce both K_1 and K_2.[31] Evidence that MRG is a zero-moment half metal comes from the x-dependence of the moment, the exceptionally large anomalous Hall effect and the electronic structure calculations with electronic doping. The room-temperature spin polarization, on which the success of spintronic applications will depend, should be improved by further composition and process optimization.

An early goal is to optimize tunnel magnetoresistance. Our preliminary work shows a TMR of $\sim 40\,\%$ in perpendicular MTJs with an MgO barrier,[31] with good prospects for improvement. Mn diffusion into the barrier is a problem that may be resolved by using Ta or Mo insertion layers. Current values of K_1 are compatible with $K_1V/kT \geq 50$ for pillars 16 nm in diameter and 30 nm thick. Spin-transfer torque switching of MRG has yet to be demonstrated. Most interesting, perhaps, is the prospect of using MRG as resonant layer in spin-torque oscillators with crossed anisotropy.[32] It should be possible to tune the resonance in the range from hundreds of GHz up to 2 THz,[33] opening the prospect of spintronic chip-to-chip communications in the THz range.

MRG is unlikely to be unique. Other compensated pseudocubic Heusler films with an electron count that places the Fermi energy in a spin gap can probably be found. The challenge of identifying and experimentally characterising new candidate materials can be met only with the aid of

high-throughput calculations, combined with a strong experimental feedback loop. There is much work to be done to realize this potential and exploit the benefits of this new class of materials for spin electronics.

This work was supported by Science Foundation Ireland through AMBER, and from Grant No. 13/ERC/I2561. K.R. acknowledges financial support from the European Community's Seventh Framework Programme IFOX, NMP3-LA-2010-246102. D.B. acknowledges financial support from IRCSET. M.Z. and T.A. acknowledge support from FP7 project 'ROMEO' (grant number 309729). The X-ray absorption measurements were performed on the EPFL/PSI X-Treme beamline at the Swiss Light Source, Paul Scherrer Institut, Villigen, Switzerland. The authors would like to thank H. Kurt for fruitful discussions.

[1] J. M. D. Coey and S. Sanvito, Journal of Physics D: Applied Physics **37**, 988 (2004).
[2] M. I. Katsnelson, V. Y. Irkhin, L. Chioncel, A. I. Lichtenstein, and R. A. de Groot, Rev. Mod. Phys. **80**, 315 (2008).
[3] A. Hirohata, H. Sukegawa, H. Yanagihara, I. Zutic, T. Seki, S. Mizukami, and R. Swaminathan, Magnetics, IEEE Transactions on **51**, 1 (2015).
[4] P. Mavropoulos, I. Galanakis, V. Popescu, and P. H. Dederichs, Journal of Physics: Condensed Matter **16**, S5759 (2004).
[5] K. Özdoğan and I. Galanakis, Journal of Applied Physics **110**, 076101 (2011).
[6] M. Vahidi, J. A. Gifford, S. K. Zhang, S. Krishnamurthy, Z. G. Yu, L. Yu, M. Huang, C. Youngbull, T. Y. Chen, and N. Newman, APL Materials **2**, 046108 (2014).
[7] S. Tsunegi, Y. Sakuraba, M. Oogane, K. Takanashi, and Y. Ando, Applied Physics Letters **93**, 112506 (2008).
[8] N. Tezuka, N. Ikeda, F. Mitsuhashi, and S. Sugimoto, Applied Physics Letters **94**, 162504 (2009).
[9] J. M. D. Coey and M. Venkatesan, Journal of Applied Physics **91**, 8345 (2002).
[10] R. A. de Groot, F. M. Mueller, P. G. v. Engen, and K. H. J. Buschow, Phys. Rev. Lett. **50**, 2024 (1983).
[11] X. Hu, Advanced Materials **24**, 294 (2012).
[12] S. Wurmehl, H. C. Kandpal, G. H. Fecher, and C. Felser, J. of Phys.: Cond. Matter **18**, 6171 (2006).
[13] H. Kurt, K. Rode, P. Stamenov, M. Venkatesan, Y.-C. Lau, E. Fonda, and J. M. D. Coey, Phys. Rev. Lett. **112**, 027201 (2014).
[14] E. Şaşıoğlu, Phys. Rev. B **79**, 100406 (2009).
[15] T. Graf, C. Felser, and S. S. Parkin, Progress in Solid State Chemistry **39**, 1 (2011).
[16] P. Klaer, M. Kallmayer, H. J. Elmers, L. Basit, J. Thöne, S. Chadov, and C. Felser, Journal of Physics D: Applied Physics **42**, 084001 (2009).
[17] D. Betto, N. Thiyagarajah, Y.-C. Lau, C. Piamonteze, M.-A. Arrio, P. Stamenov, J. M. D. Coey, and K. Rode, Phys. Rev. B **91**, 094410 (2015).
[18] K. Rode, N. Baadji, D. Betto, Y.-C. Lau, H. Kurt, M. Venkatesan, P. Stamenov, S. Sanvito, J. M. D. Coey, E. Fonda, E. Otero, F. Choueikani, P. Ohresser, F. Porcher, and G. André, Phys. Rev. B **87**, 184429 (2013).
[19] L. Wollmann, S. Chadov, J. Kübler, and C. Felser, Phys. Rev. B **90**, 214420 (2014).
[20] T. Hori, M. Akimitsu, H. Miki, K. Ohoyoama, and Y. Yamaguchi, Applied Physics A **74**, s737 (2002).
[21] N. Nagaosa, Journal of the Physical Society of Japan **75**, 042001 (2006), http://dx.doi.org/10.1143/JPSJ.75.042001.
[22] N. Nagaosa, J. Sinova, S. Onoda, A. H. MacDonald, and N. P. Ong, Rev. Mod. Phys. **82**, 1539 (2010).
[23] N. Thiyagarajah, Y.-C. Lau, D. Betto, K. Borisov, J. M. D. Coey, P. Stamenov, and K. Rode, Applied Physics Letters **106**, 122402 (2015).
[24] J. W. F. Dorleijn, Philips Res. Rep. **31** (1976).
[25] T. W. Kim, S. H. Lim, and R. J. Gambino, J. of Appl.Phys. **89**, 7212 (2001).
[26] T. Jungwirth, Q. Niu, and A. H. MacDonald, Phys. Rev. Lett. **88**, 207208 (2002).
[27] Y. Pu, D. Chiba, F. Matsukura, H. Ohno, and J. Shi, Phys. Rev. Lett. **101**, 117208 (2008).
[28] M. Zic, K. Rode, N. Thiyagarajah, Y.-C. Lau, D. Betto, J. M. D. Coey, S. Sanvito, K. J. O'Shea, C. A. Ferguson, and D. A. MacLaren, arXiv:1511.07923 (2015).
[29] I. Galanakis, K. Özdoğan, E. Şaşıoğlu, and S. Blügel, Journal of Applied Physics **116**, 033903 (2014).
[30] http://www.materials-mine.com.
[31] C. Fowley, unpublished (2015).
[32] M. Gensch, unpublished (2016).
[33] The resonance frequency is given by $\omega_r = \mu_0\gamma\sqrt{H'_a(2H_{ex}+H'_a)} \approx \mu_0\gamma\sqrt{2H'_aH_{ex}}$ for an antiferromagnetic sample, where $H'_a = 2K_u/M_{sl}$ (M_{sl} is the sublattice magnetization) and γ is the gyromagnetic ratio. We estimate the exchange field to be μ_0H_{ex} = 890 T and the sublattice anisotropy field is approximately $\mu_0H'_a$ = 0.4 T. The resonance frequency is of order 0.75 THz.